AIP | The Journal of Chemical Physics

Infrared spectra of cis and trans-(NO)2− anions in solid argon

Lester Andrews, Mingfei Zhou, Stephen P. Willson, Gary P. Kushto, Anders Snis et al.

Citation: J. Chem. Phys. **109**, 177 (1998); doi: 10.1063/1.476547
View online: http://dx.doi.org/10.1063/1.476547
View Table of Contents: http://jcp.aip.org/resource/1/JCPSA6/v109/i1
Published by the American Institute of Physics.

Infrared spectra of *cis* and *trans*-$(NO)_2^-$ anions in solid argon

Lester Andrews, Mingfei Zhou, Stephen P. Willson, and Gary P. Kushto
Department of Chemistry, University of Virginia, Charlottesville, Virginia 22901

Anders Snis and Itai Panas
Department of Inorganic Chemistry, Göteborg University, 5-41296 Göteborg, Sweden

(Received 3 February 1998; accepted 27 March 1998)

Laser-ablation of over 20 different metal targets with concurrent 10 K codeposition of Ar/NO mixtures produces metal independent infrared bands at 1589.3 cm^{-1} due to $(NO)_2^+$, a new absorption at 1221.0 cm^{-1}, and a band set at 1300.3, 1222.7, 884.4 cm^{-1}. The latter bands decrease more on annealing than the 1221.0 cm^{-1} band. Isotopic substitution (^{14}NO, ^{15}NO, $^{15}N^{18}O$, and mixtures) shows that these new vibrations involve two equivalent N–O oscillators, which identifies two new $(NO)_2$ species. The excellent agreement with frequencies, intensities, and isotopic frequency ratios from density functional theory calculations substantiates assignment of the 1221.0 cm^{-1} band to *trans*-$(NO)_2^-$ and the three band set to *cis*-$(NO)_2^-$. The observation of a weak combination band at 2492.0 cm^{-1} further substantiates assignment of the two N–O stretching modes in *cis*-$(NO)_2^-$. © *1998 American Institute of Physics.* [S0021-9606(98)02525-2]

INTRODUCTION

Nitrogen oxides are byproducts of fuel combustion using air as the oxidant, and their catalytic removal involves reduction on a metal surface where anionic species may be involved.[1] An important and structurally interesting anion is $N_2O_2^-$, which can exist in *cis*, *trans*, and C_{2v} forms. Evidence for different $N_2O_2^-$ structures has been presented in recent negative ion photoelectron investigations.[2–4] Three matrix isolation studies have also provided information on $N_2O_2^-$ anions. In the first study, mercury arc photolysis of matrix isolated N_2O in the presence of alkali metal atoms gave $(NO)_2$ and the NNO_2^- anion.[5] The next investigation employed chemical ionization of argon/N_2O mixtures[6] and observed the NNO_2^- anion, and a new absorption at 1590 cm^{-1}, which was first assigned to $(NO)_2^-$ but was subsequently reassigned to $(NO)_2^+$ on the basis of gas phase ZEKE photoelectron spectroscopic studies.[7] The last work employed discharged neon and observed neon matrix counterparts of the above and other charged species.[8,9]

We are currently investigating the reaction of laser-ablated metal atoms with NO in condensing argon.[10–12] Electrons produced in the ablation process can be captured by molecules during condensation in excess argon, thus metal-independent absorptions must be considered for isolated anions in these experiments. In this manner, isolated O_4^- has been observed in metal experiments with dioxygen.[13–17] We report here evidence for the *cis* and *trans* structural isomers of $(NO)_2^-$ and a more weakly bound asymmetric $(ON)(ON)^-$ complex in these experiments.

A parallel combined *ab initio* quantum chemistry and density functional theory study explores how excess electrons affect the homogeneous and heterogeneous nitric oxide chemistry.[18–20] An extra electron fosters the formation of an intermolecular N–N bond with bond order 1.5, and the resulting anion is 1.7 eV below the $2NO+e^-$ asymptote. The dimer anion stability and characteristic frequencies at different CaO surface sites were also determined recently, stressing the possible importance of this transient to efficient catalytic NO reduction.[20]

Agreement is found between the elaborate Coupled Cluster CCSD(T) and Complete Active Space Second Order Perturbation Theory CASPT2 methods as well as with the computationally more handy B3LYP hybrid density functional in predicting *trans*-$(NO)_2^-$ to be most stable, followed by the *cis* and the NNO_2^- structures, about 3 and 6 kcal/mol higher, respectively. This stability ordering is contrary to that reported at the Hartree–Fock level of theory.[21] The latter calculation was repeated and restricted open-shell Hartree–Fock (ROHF) was found to be unique in this prediction, possibly due to failure to describe electron correlation effects.[18] Vibrational frequencies were estimated for several dimer structures at the B3LYP/6-31$G(d)$ level to qualitatively estimate the bond order in the N–N dimer bond.

EXPERIMENT

Pulsed-laser ablated metal atoms and electrons were codeposited with Ar/NO (^{14}NO, ^{15}NO, or $^{15}N^{18}O$) mixtures on a 7 or 10 K optical surface as described in previous reports.[10–16,22] The 1064 nm fundamental of a Nd–YAG laser was focused on the metal target to a spot about 0.2 mm in diameter using 10–40 mJ pulses of 10 ns duration such that a visible plume above the target was observed; lower laser energy (and lower plume intensity) favored the stabilization of anion species. Infrared spectra were recorded on Nicolet 550 or 750 spectrometers at 0.5 cm^{-1} resolution and ± 0.1 cm^{-1} accuracy using a liquid nitrogen cooled MCTB detector. Samples were annealed from 7 or 10 K and subjected to broadband photolysis and more spectra were recorded.

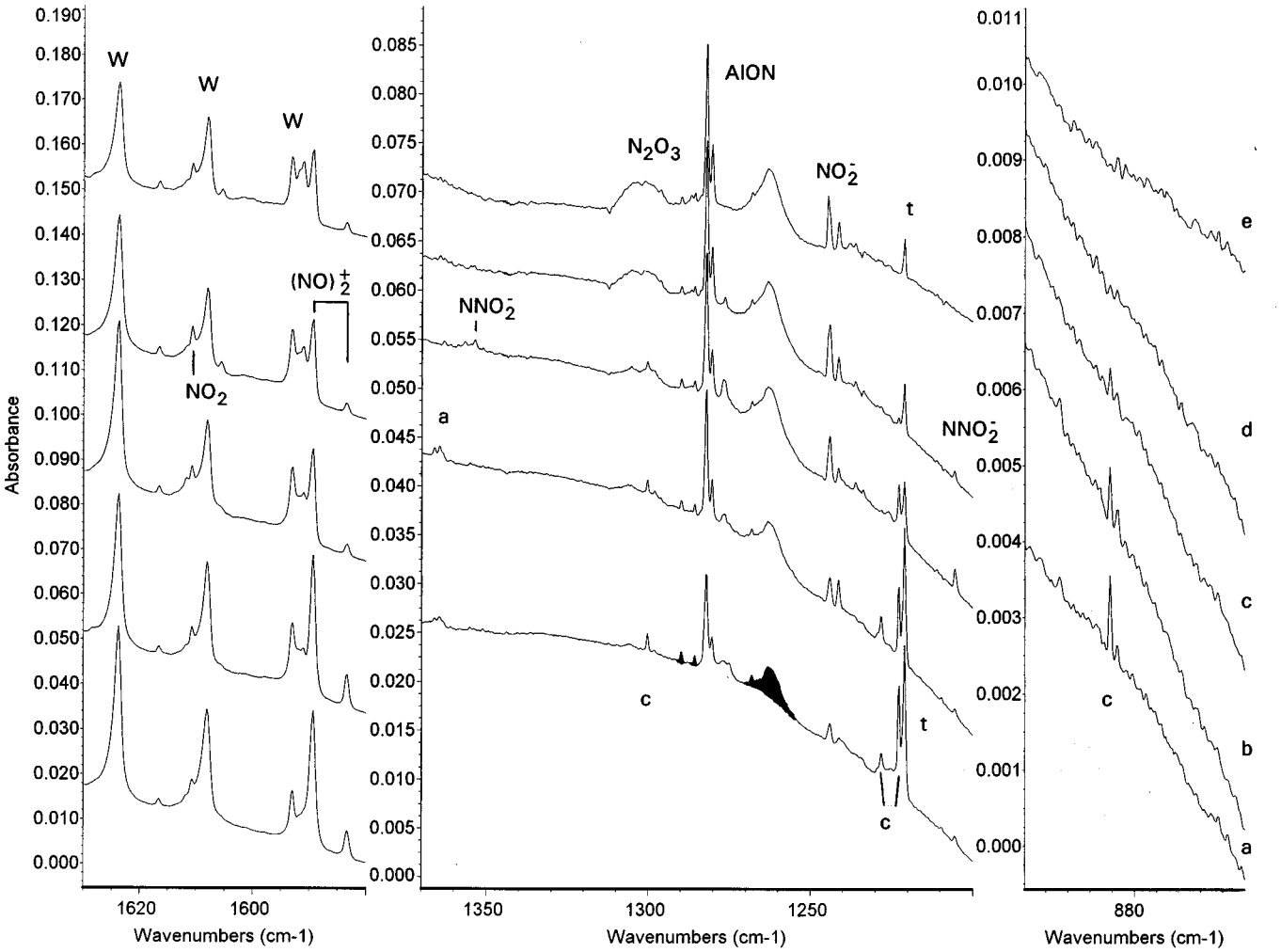

FIG. 1. Infrared spectra in the 1630–1580, 1370–1200, and 900–860 cm^{-1} region for laser-ablated Al and electrons codeposited at 10 K with 0.3% NO in excess argon. (a) Sample codeposited for 1.5 h, (b) after annealing to 25 K, (c) after broadband photolysis for 30 min, (d) after annealing to 30 K, and (e) after annealing to 35 K. The ''blackened'' bands in the 1290–1250 cm^{-1} region are in the sample codeposited without aluminum. Note that the noise level in the 800 cm^{-1} region is approximately 1×10^{-4} absorbance units.

RESULTS

The absorptions reported here are common (within ±0.1 cm^{-1}) to over 20 different metal studies and are due to reaction products involving the common reagent, namely electrons, produced in the laser ablation process. Figure 1 shows spectra from the 1630–1580, 1370–1200, and 900–860 cm^{-1} regions using an aluminum target, and Table I gives the product absorptions. Deposition at 10 K reveals strong NO and $(NO)_2$ absorptions, weak N_2O and N_2O_3 bands (not shown),[23,24] water bands (labeled W), weak NO_2 at 1610.8 cm^{-1}, $(NO)_2^+$ at 1589.3 and 1583.4 cm^{-1},[6–8] a sharp, weak 1364.4 cm^{-1} band (labeled *a*), AlON at 1282.1 cm^{-1},[10] NO_2^- at 1243.7 cm^{-1}, NNO_2^- at 1205.3 cm^{-1},[5,6] a sharp new band at 1221.0 cm^{-1} (labeled *t*) with satellites at 1222.7 and 1228.1 cm^{-1} (labeled *c*), and sharp weak new bands at 1300.4 and 884.4 cm^{-1} (labeled *c*). Annealing to 25 K slightly increases the N_2O, NO_2, 1364.4 cm^{-1}, and NO_2^- absorptions, but decreases the 1221.0 and 1205.3 cm^{-1} bands by 10%, and the 1300.3, 1222.7, and 884.4 cm^{-1} band set by 20%, while the ''*c*'' satellites at 1298.2, 1228.1, and 883.2 cm^{-1} increase by

TABLE I. Infrared absorptions (cm^{-1}) in laser-ablated metal matrix isolation experiments with argon/nitric oxide mixtures at 10 K.

$^{14}N^{16}O$	$^{15}N^{16}O$	$^{15}N^{8}O$	ident
3608.6	3545.3	3450.4	*c*-$(NO)_2$
2492.0	2447.4	2386.3	*c*-$(NO)_2^-$
1871.8	1838.8	1789.2	NO
1863.3	1830.5	1781.2	*c*-$(NO)_2$
1776.2	1744.7	1697.5	*c*-$(NO)_2$
1589.3	1561.9	1520.3	$(NO)_2^+$
1583.4	1556.0	1514.6	$(NO)_2^+$ site
1364.4	1341.5	1305.2	$(ON)(ON)^-$
1300.3	1278.9	1242.7	*c*-$(NO)_2^-$
1298.2	1276.8	1240.5	*c*-$(NO)_2^-$ site
1243.7	1218.3	1191.9	NO_2^-
1241.2	1215.9	1189.7	NO_2^- site
1228.1	1203.9	1177.1	*c*-$(NO)_2^-$ site
1222.7	1198.6	1172.0	*c*-$(NO)_2^-$
1221.0	1199.9	1167.4	*t*-$(NO)_2^-$
1205.3	1181.5	1155.5	NNO_2^-
884.4	866.1	847.8	*c*-$(NO)_2^-$
883.2	864.9	846.6	*c*-$(NO)_2^-$ site

TABLE II. Photochemical and annealing behavior of selected infrared absorptions (cm^{-1}) in a thulium experiment with 0.3% NO in argon.

	$(ON)(ON)^-$ 1364.1	NO_2^- 1243.7	*cis*-$(NO)_2^-$ 1222.7	*trans*-$(NO)_2^-$ 1221.0	NNO_2^- 1205.3
Sample	7.0[a]	18.9	2.3	21.6	3.0
490–580 nm	5.0	22.9	2.9	19.3	3.0
380–580 nm	0.0	31.2	5.0	13.9	3.0
240–580 nm	0.0	28.9	2.2	3.2	3.9
25 K	0.0[b]	28.9	7.2	3.2	3.9
30 K	0.0	24.7	2.2	3.2	2.9

[a]Integrated areas: (absorbance units$\times cm^{-1}$)$\times$1000 to simplify table.
[b]In $^{15}N^{18}O$ experiment 20% of the original 1305.1 cm^{-1} band destroyed on photolysis reappears on 25 K annealing.

about 30% [Fig. 1(b)]. Broadband photolysis (medium pressure mercury arc, 240–580 nm) destroys the ''*a*'' band, markedly decreases the $(NO)_2^+$ bands and the latter sharp new ''*t*'' and ''*c*'' absorptions, and increases the NNO_2^- bands at 1353.6 and 1205.3 cm^{-1} [Fig. 1(c)].[5,6,9] A very weak 2492.0 cm^{-1} band ($A=0.0003$ absorbance units, a.u., not shown) tracks with the ''*c*'' band set on annealing and on photolysis. Annealing to 30 and 35 K decreases the 1221.0 cm^{-1} band but destroys the 1300.3, 1222.7, and 884.4 cm^{-1} band set; the 1364.4 cm^{-1} band reappears weakly then disappears on these annealing cycles. Similar experiments with thulium give more ''*t*'' at 1221.0 cm^{-1} relative to ''*c*'' at 1222.7 cm^{-1} and the weak new band at 1364.1 cm^{-1}. Selective photolysis at 490–580, 390–580, and 240–580 nm destroys the 1364.1 cm^{-1} band, increases in stages the 1222.7 cm^{-1} ''*c*'' band and its associated 1300.3 and 884.4 cm^{-1} bands, decreases the 1221.0 cm^{-1} ''*t*'' band, and increases the 1205.3 cm^{-1} NNO_2^- absorption. These changes are summarized in Table II.

The 1221.0 cm^{-1} band shifted to 1199.9 cm^{-1} with ^{15}NO and the sharp latter set to 1278.9, 1198.6, and 866.1 cm^{-1} while the weak 1364.4 cm^{-1} absorption shifted to 1341.5 cm^{-1} and the very weak 2492.0 cm^{-1} band shifted to 2447.4 cm^{-1}. Again the latter trio decreased to a greater degree on annealing than the 1199.9 cm^{-1} band. These bands and satellites are given in Table I. Figure 2 shows the inter-

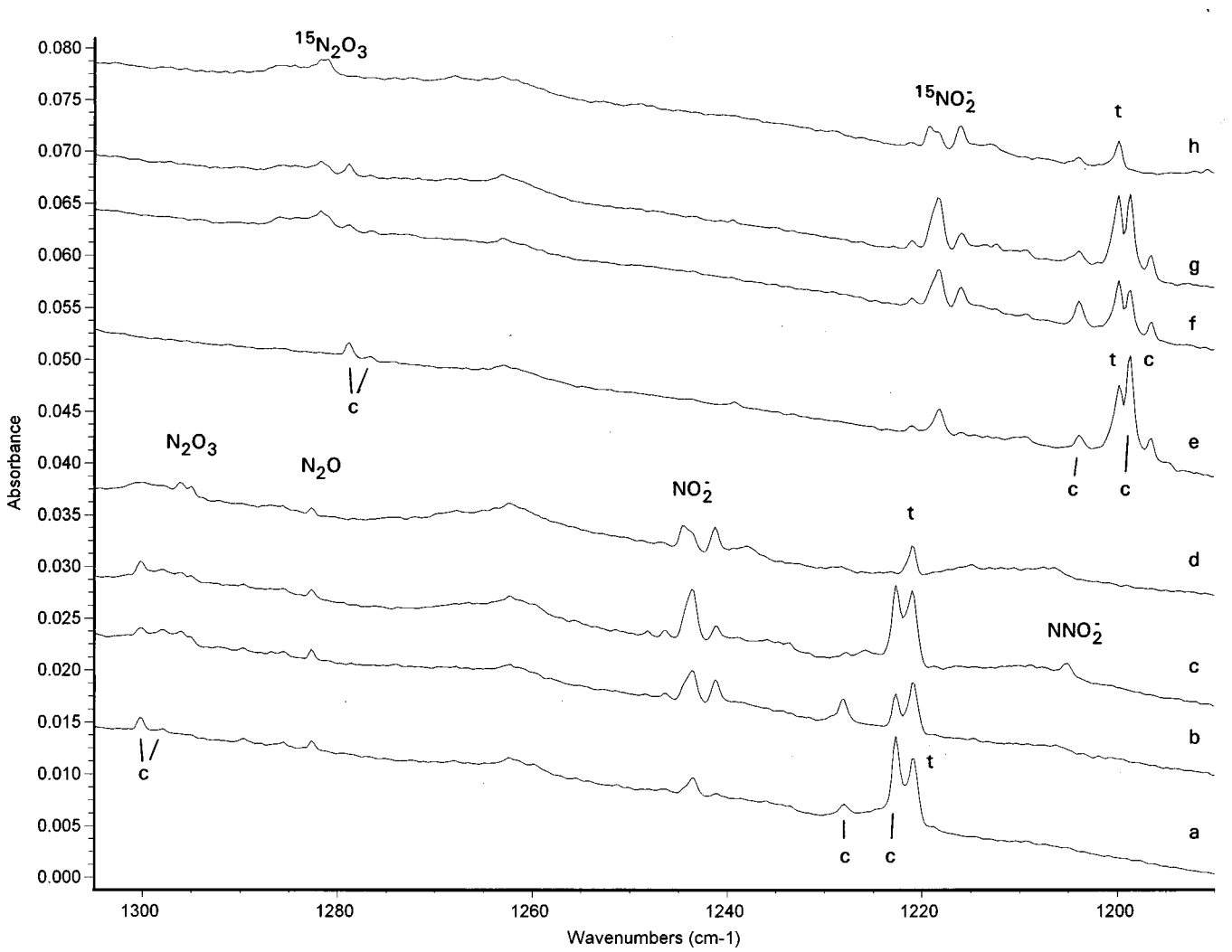

FIG. 2. Infrared spectra in the 1305–1190 cm^{-1} region for laser-ablated Pr and electrons codeposited at 7 K with 0.2% isotopic nitric oxide in argon. (a) ^{14}NO sample codeposited for 1 h, (b) after 25 K annealing, (c) after broadband photolysis, (d) after 33 K annealing, (e) ^{15}NO sample codeposited for 1 h, (f) after 25 K annealing, (g) after broadband photolysis, and (h) after 33 K annealing.

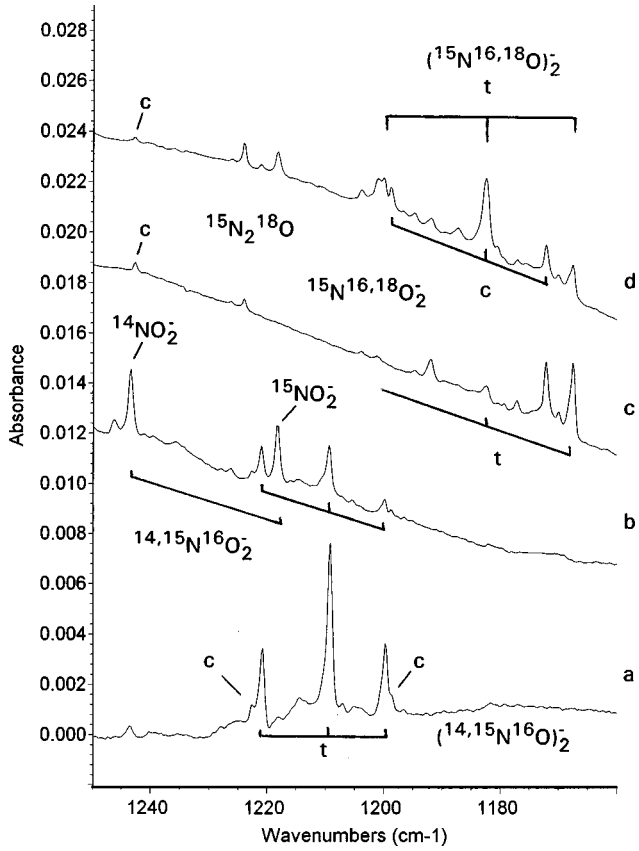

FIG. 3. Infrared spectra of NO isotopic mixtures (0.3%) in argon condensed at 10 K with laser ablated metals. (a) $^{14}NO+^{15}NO+Er$, (b) $^{14}NO+^{15}NO+Fe$, (c) $^{15}N^{16}O+^{15}N^{18}O+V$, and (d) $^{15}N^{16}O+^{15}N^{18}O+Sc$.

play between the ''*c*'' and ''*t*'' bands using a praseodymium target and ^{14}NO or ^{15}NO in argon. As with aluminum, annealing to 25 K increased one ''*c*'' site at the expense of the other site, but photolysis reversed this process. Sharp 884.4, 883.2, and 866.1, 864.9 cm^{-1} bands (not shown) followed accordingly. On final annealing to 33 K only the ''*t*'' species survives. The 1199.9 cm^{-1} band shifted to 1167.4 cm^{-1} with $^{15}N^{18}O$ and the sharp trio to 1242.7, 1172.0, and 847.8 cm^{-1} with analogous annealing behavior, while the 1341.5 cm^{-1} absorption shifted to 1305.2 cm^{-1} and the very weak 2447.4 cm^{-1} band shifted to 2386.3 cm^{-1}. The relative yield of the ''*a*,'' ''*c*,'' and ''*t*'' bands was higher in experiments using lanthanum and yttrium with NO isotopic molecules.

Spectra of isotopic mixtures are complicated by the presence of NO_2^- in the same spectral region, but different metal targets give different populations of the new band sets and NO_2^-. Figure 3 contrasts mixed $^{14}NO+^{15}NO$ experiments using erbium and iron targets: note the $^{14,15}NO_2^-$ doublet at 1243.7 and 1218.3 cm^{-1} and the 1221.0, 1209.4, and 1199.9 cm^{-1} triplet for the new ''*t*'' band. Figure 3 also compares mixed $^{15}N^{16}O+^{15}N^{18}O$ samples with vanadium and scandium targets: different ^{18}O enrichments aid identification of the $^{15}N^{16,18}O_2^-$ triplet at 1218.3, 1201.1, and 1191.9 cm^{-1} and the new ''*t*'' triplet at 1199.9, 1182.4, and 1167.4 cm^{-1}. Clearly, the new 1221.0 cm^{-1} absorption is due to a species with two equivalent N and two equivalent O atoms and a new $(NO)_2^q$ species is thus identified.

The weaker 1364.4 cm^{-1} band is difficult to observe in mixed isotope experiments. Three $^{14}NO+^{15}NO$ experiments were done with chromium and 0.3%, 0.8%, and 1% total NO concentrations to optimize the yield. The 1364.4 cm^{-1} band shifts to 1341.5 cm^{-1} with ^{15}NO and these absorptions become a 1:1:1:1 quartet at 1364.4, 1362.2, 1344.5, and 1341.5 cm^{-1} with the mixture. This quartet increases slightly on annealing to 25 and 30 K, decreases on annealing to 35 K, and vanishes on 240–580 nm photolysis.

While the spectra in Fig. 3 are selected to maximize the relative yield of the ''*t*'' bands, the mixed isotopic spectra in Figs. 4 and 5 are chosen to maximize the ''*c*'' bands. Note that the major ''*c*'' band appears at 1222.7 cm^{-1}, above the ''*t*'' band at 1221.0 cm^{-1} for the $^{14}N^{16}O$ isotope, but these positions are reversed for the $^{15}N^{16}O$ isotopic species with ''*t*'' at 1199.9 cm^{-1} and ''*c*'' at 1198.6 cm^{-1}. Figure 4 shows spectra for a ^{14}NO, ^{15}NO mixture using a cerium target; sharp triplets are observed at 1300.3, 1291.2, and 1278.9 cm^{-1} and 884.4, 875.6, and 866.0 cm^{-1} for the upper and lower ''*c*'' bands; the 1200–1220 cm^{-1} region yields a single intermediate mixed isotopic band at 1209.3 cm^{-1} for both ''*c*'' and ''*t*'' species because of the above described relationship between ''*c*'' and ''*t*'' on substitution of ^{15}NO for ^{14}NO. On 25 K annealing, the second ''*c*'' site grows at the expense of the first ''*c*'' band, and the intermediate mixed ^{14}NO, ^{15}NO component appears at 1214.7 cm^{-1} [Fig. 4(b)]. Note the slight asymmetry in this ''*c*'' site triplet: the 1214.7 cm^{-1} band is 1.3 cm^{-1} *below* the pure isotopic ''*c*'' site median whereas the upper intermediate band at 1289.1 cm^{-1} is 1.6 cm^{-1} *above* the pure isotopic band median.

Figure 5 shows analogous spectra for a $^{15}N^{16}O$, $^{15}N^{18}O$ mixture using a samarium target; sharp triplets were observed at 1278.9, 1263.8, and 1242.7 cm^{-1} and 866.1, 856.9, and 847.7 cm^{-1} for the two weaker ''*c*'' bands; again because of the reversal in ''*c*'' and ''*t*'' band positions from $^{15}N^{16}O$ to $^{15}N^{18}O$, a single central mixed isotopic component is observed at 1182.5 cm^{-1}. On 25 K annealing, the second ''*c*'' site is favored and the intermediate mixed $^{15}N^{16}O$, $^{15}N^{18}O$ component is resolved at 1187.3 cm^{-1} [Fig. 5(b)]. Again note the asymmetry in this triplet: the 1187.3 cm^{-1} band is 3.2 cm^{-1} *below* the pure isotopic ''*c*'' site median while the upper intermediate band at 1261.6 cm^{-1} is 3.0 cm^{-1} *above* the pure isotopic band median. The triplet structures for the ''*c*'' bands indicate that this absorbing species also contains two equivalent N and two equivalent O atoms, and the matching asymmetries for the two upper bands further associate these absorptions with the same molecular species.

Several experiments were done by depositing NO (0.3%) in argon with a glow discharge maintained through the depositing sample on the window surface using an electrode similar to that described previously.[25] With 300 V dc between the electrode and copper block, no discharge is observed, but laser ablation of a metal target *below the visible emission threshold* provides enough electrons to initiate the discharge that is maintained by the dc potential. Similar discharge experiments have been done to enhance anion species

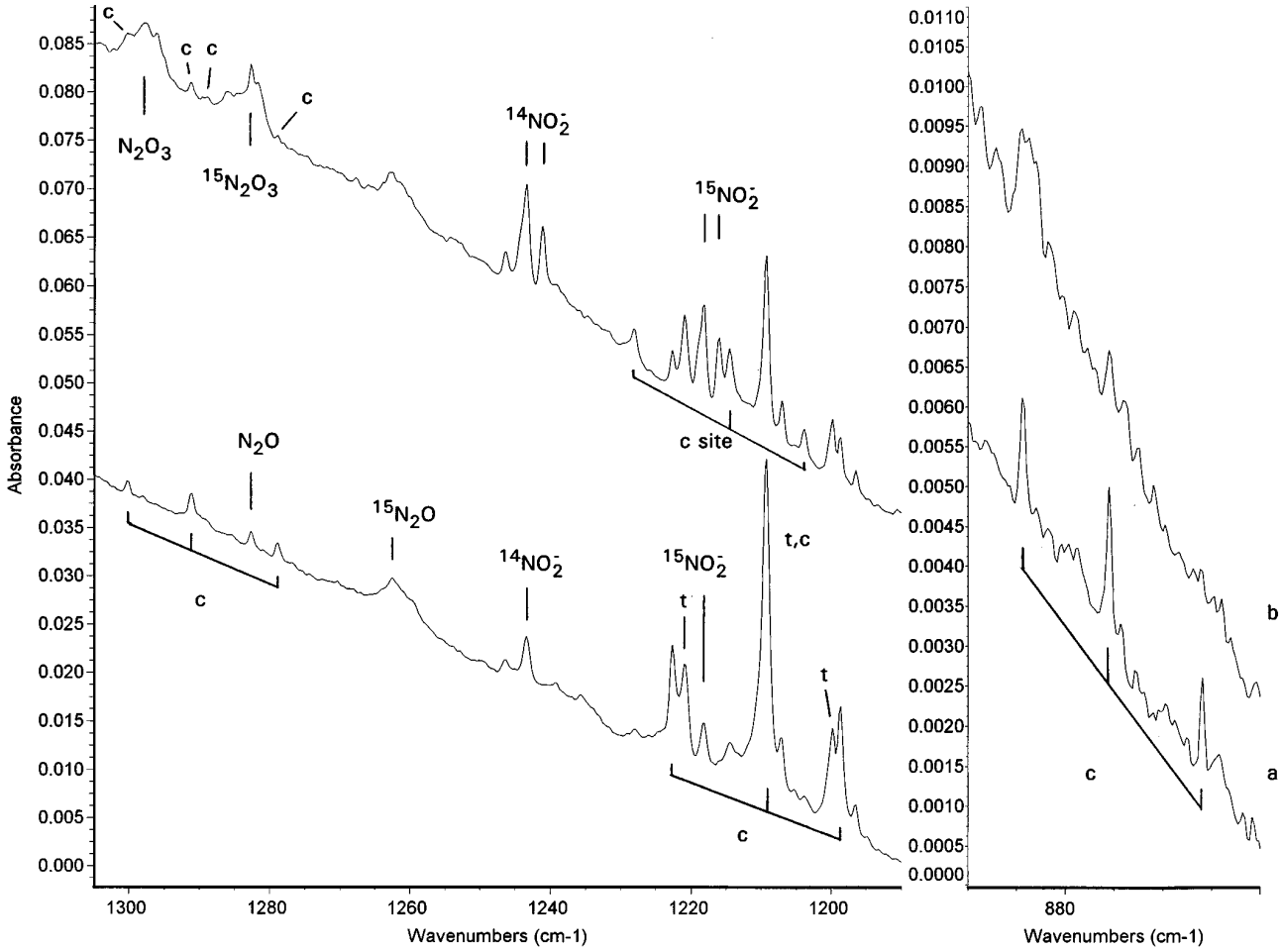

FIG. 4. Infrared spectra of $^{14}NO+^{15}NO$ mixture in argon (total 0.3% NO) condensed at 7 K with laser ablated Ce. (a) Sample condensed at 10 K for 1 h, and (b) after annealing to 25 K.

in thallium experiments.[26] In addition to NO, $(NO)_2$, and weak N_2O_3 absorptions, strong $(NO)_2^+$ and NO_2^- bands were observed along with the same sharp ''*c*'' and ''*t*'' absorptions. The absorbance yield was about twice that in Fig. 1 and the yield of the ''*c*'' bands was increased relative to the ''*t*'' band including the weak 2492.0 cm^{-1} band. With ^{15}NO the ''*c*'' bands were again enhanced including the weak 2447.4 cm^{-1} band, and, as described above, the strong ''*c*'' and ''*t*'' band positions reverse on ^{15}NO substitution. Very weak metal reaction products were observed in these experiments, less than 10% of the yield using the laser power normally employed here. The experiment was continued with normal laser power, and the metal products increased markedly whereas the $(NO_2)^+$, NO_2^-, ''*t*,'' and ''*c*'' bands increased a much smaller proportion.

Following quantum chemical calculations on the $(NO)_2^-$ anion system,[18] isotopic frequencies have been calculated at the DFT/B3LYP[27] level using the $6-311+G(d)$ basis set for the lowest energy doublet state of the three anion structures. The isotopic modifications listed in Table III were considered, and the Gaussian program package was employed.[28] Structures for these anions are given in Table 1 of Ref. 18. One main achievement of the Snis–Panas studies was to demonstrate the B3LYP functional predictive power for $(NO)_2^-$ anions. Structures and stabilities are in agreement with CASPT2 calculations. Also, frequencies determined by the regularized CASSCF method reg-CASSCF,[29] using the MOLCAS program package,[29] and B3LYP are in qualitative agreement.[20] The calculations are exploited in the present study to correlate infrared (IR) intensities and frequencies for isotopically labeled $(NO)_2^-$ anions. Parameters have also been calculated at the same level of theory for NO (1980.5 cm^{-1}, 46 km/mol, 1.148 Å) and NO^- (1415.6 cm^{-1}, 134 km/mol, 1.264 Å).[20] Note that the calculated NO frequency is 5.8% higher than the 1871.8 cm^{-1} solid argon value.

Qualitative discrepancy between explicit wave-function-based quantum chemistry and density functional theory (DFT) is known to occur for loosely bound systems and systems which simultaneously display important local and nonlocal qualities. The weakly bound (about 4 kcal/mol) quartet state $(ON)(ON)^-$ anion complex is understood to be one such system, i.e., DFT delocalizes the excess charge over the entire complex while a reg-CASSCF treatment, which has all the electron configurations produced by distributing 15 electrons in the 12 atomic $2p$ orbitals, localizes the extra electron on one of the monomers. As the scenario displayed by the reg-CASSCF treatment is understood to be the more physical, only reg-CASSCF computational results for the $(ON)(ON)^-$ system will be referred to when comparing

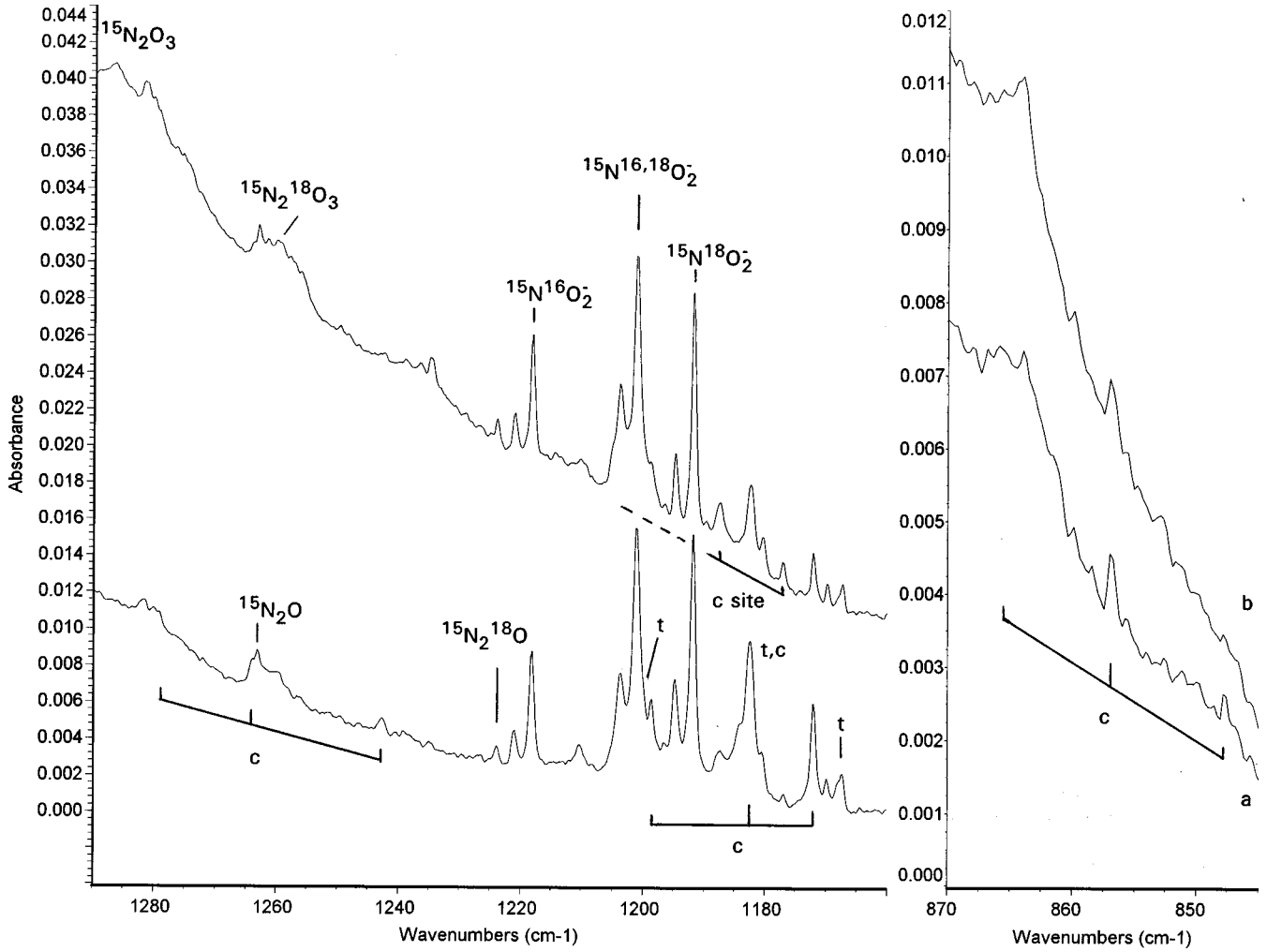

FIG. 5. Infrared spectra of $^{15}N^{16}O+^{15}N^{18}O$ mixture in argon (total 0.3% NO) condensed at 7 K with laser ablated Sm. (a) Sample condensed at 10 K for 1 h, and (b) after annealing to 25 K.

to experiment. Table IV collects frequencies and bond lengths for NO, NO^-, and $(ON)(ON)^-$ calculated at the reg-CASSCF level, using the Atomic Natural Orbital basis set of Pierloot *et al.*[30] with $5s$, $4p$, and $2d$ functions for nitrogen and oxygen.

DISCUSSION

The photosensitive nature of the new 1221.0 cm^{-1} band and the 1300.3, 1222.7, and 884.4 cm^{-1} band set with satellite set at 1298.2, 1228.1, and 883.2 cm^{-1} and their net reduction on annealing suggest a new transient species. The observation of these bands using over 20 different metal targets shows that either electrons or photons from the laser-induced target emission plume are responsible for the processes through which NO is converted into the new species ''*t*'' and ''*c*.''

Identification

The mixed isotopic spectra clearly show triplet absorption patterns, which means that both species ''*t*'' and ''*c*'' involve two equivalent N atoms and two equivalent O atoms, and starting with NO, most probably two equivalent NO submolecules. Hence, we must consider $(NO)_2^q$ species. The strong 1590 cm^{-1} (here 1589.3 cm^{-1}) band was first identified as a $(NO)_2^q$ species from isotopic shifts and splittings, and q was presumed to be -1 because of the photosensitive nature of the absorptions in parallel with O_3^- and NO_2^- behavior.[6] Later gas phase ZEKE photoelectron investigations[7] observed the same vibrational intervals as in a solid neon matrix[7,8] and reassigned q as $+1$. Since the present ''*t*'' and ''*c*'' bands are lower in frequency, they are reasonable candidates for the anion species, particularly in view of the very recent prediction from DFT/B3LYP calculations of the strongest infrared absorption for *cis*- and *trans*-$(NO)_2^-$ near 1300 cm^{-1} using the 6-31$G(d)$ basis set.[18]

Assignments

Table III lists the *cis*- and *trans*-$(NO)_2^-$ frequencies calculated again with the larger 6-311+$G(d)$ basis set. Note that the strongest infrared bands predicted for the *cis* anion isomer (1287.8 cm^{-1}) and the *trans* anion isomer (1267.5 cm^{-1}) are just 4%–5% higher than the strongest ''*c*'' and ''*t*'' bands observed here.

Of more importance, however, is the comparison of observed isotopic frequency ratios, as a characteristic of the

TABLE III. Frequencies (cm^{-1}) and infrared intensities (km/mol) calculated for the *trans*, *cis*, and C_{2v} structures of $(NO)_2^-$ anions for $^{14}N^{16}O$, $^{15}N^{16}O$, and $^{15}N^{18}O$ isotopic modifications using Gaussian 94 DFT/B3LYP and 6-311+$G(d)$ basis set.

	trans-$(NO)_2^-(^2A_u)$			*cis*-$(NO)_2^-(^2B_1)$			$C_{2v}NNO_2^-(^2B_2)$		
Isotope	Freq	Mode	Int	Freq	Mode	Int	Freq	Mode	Int
	1334.0	a_g	0	1353.9	a_1	51	1360.5	a_1	202
	1267.5	b_u	401	1287.8	b_2	339	1235.5	b_2	396
14–16	792.6	a_g	0	921.3	b_2	50	1043.0	a_1	44
	678.3	a_g	0	735.0	a_1	5	772.7	b_1	6
	508.6	b_u	66	395.8	a_1	0.6	644.4	a_1	0.2
	334.7	a_u	3	164.0	a_2	0.2	534.8	b_2	6
	1307.3	a_g	0	1331.4	a_1	51	1316.4	a_1	204
	1244.8	b_u	392	1260.9	b_2	336	1209.8	b_2	381
15–16	768.5	a_g	0	901.7	b_2	45	1032.0	a_1	41
	669.3	a_g	0	710.4	a_1	5	750.5	b_1	6
	499.5	b_u	64	395.1	a_1	0.7	638.7	a_1	0.1
	328.7	a_u	3	159.6	a_2	0	524.1	b_2	6
	1276.5	a_g	0	1292.2	a_1	45	1313.4	a_1	194
	1210.8	b_u	363	1233.0	b_2	304	1182.8	b_2	361
15–18	764.2	a_g	0	881.9	b_2	48	990.9	a_1	40
	645.0	a_g	0	710.0	a_1	5	743.9	b_1	5
	485.9	b_u	60	373.5	a_1	0.5	611.3	a_1	0.3
	319.7	a_u	2	157.6	a_2	0	511.6	b_2	5

normal mode, and ratios of the calculated isotopic frequencies. Table V lists the 14–16/15–16 and 15–16/15–18 isotopic frequency ratios observed here for species ''*t*'' and ''*c*'' absorptions and the ratios for the strongest infrared band calculated from quantum chemical harmonic frequencies for the *trans* isomer and for the strongest three bands for the *cis* isomer of $(NO)_2^-$. Note that the observed *trans* ratios are slightly smaller than the calculated ratios, as is expected for normal cubic anharmonicity in the observed frequencies. Starting with the 1199.9 cm^{-1} 15–16 isotopic band to normalize the DFT calculations, 1221.8 cm^{-1} is predicted for the 14–16 band, 0.8 cm^{-1} above the observed value, and 1167.1 cm^{-1} for the 15–18 band, 0.3 cm^{-1} below the observed value, which is excellent agreement. This is clearly the antisymmetric (b_u) NO stretching mode of the *trans*-$(NO)_2^-$ anion. The DFT calculations predict the other b_u mode at 508.6 cm^{-1} with 16% of the intensity of the upper b_u band. Unfortunately the noise level at 470–500 cm^{-1} is 0.001 a.u., and we are unable to detect a signal here that would be 0.002 a.u. at best.

For the *cis* species, the highest frequency displays the same relationship, namely anharmonic observed ratios slightly smaller than calculated harmonic ratios, as do the two other frequencies with 14/15 substitution but the reverse relationship is found for 16/18 substitution. Nevertheless, all of the calculated ratios are very close to the observed ratios and sufficiently close to conclude that the present argon matrix assignments to *cis*-$(NO)_2^-$ are correct. Starting with the observed 15–16 isotopic frequencies for the three bands of *cis*-$(NO)_2^-$ to normalize the DFT calculations, the three 14–16 and the three 15–18 isotopic fundamentals are predicted within an average of 0.8 cm^{-1} of the observed values. It is clear that DFT/B3LYP/6-311+$G(d)$ calculations correctly model the observed *cis*-$(NO)_2^-$ frequencies, intensities, and normal mode descriptions. In this regard the three infrared bands at 1300.3, 1222.7, and 884.4 cm^{-1} assigned here to the symmetric (a_1) and antisymmetric (b_2) N–O bond stretching modes and the antisymmetric (b_2) O–N–N bending mode for *cis*-$(NO)_2^-$ are predicted 4%–5% too high by the DFT calculation, and with 5/34/5 relative intensities compared to observed 15/100/10 absorbances ($\times 10^{-4}$ for

TABLE IV. Frequencies and bond lengths calculated for NO, NO^-, and the $^4A'$ state of $(ON)(ON)^-$.

B3LYP/6-311+$G(d)$			
$NO(^2\Pi)$	1980.5 cm^{-1}, 1.148 Å	$NO^-(^3\Sigma)$	1415.6 cm^{-1}, 1.264 Å
	(46 km/mol)		(134 km/mol)
reg-CASSCF/5s4p2d			
NO	1965 cm^{-1}, 1.140 Å	NO^-	1436 cm^{-1}, 1.258 Å
$(ON)(ON)^-$	1960 cm^{-1}, 1.140 Å		
∠O–N–O=90.9°	122 cm^{-1}, 2.88 Å		
∠N–O–N=102.7°	1435 cm^{-1}, 1.259 Å		

TABLE V. Observed and DFT/B3LYP calculated isotopic frequency ratios for *trans*- and *cis*-$(NO)_2^-$ species.

	14–16/15–16			15–16/15–18		
	Obs	Calc	Obs site	Obs	Calc	Obs site
trans[a]	1.01758	1.01824		1.02784	1.02808	
cis[b]	1.01673	1.01690	1.01676	1.02913	1.03034	1.02926
	1.02011	1.02133	1.02010	1.02270	1.02263	1.02277
	1.02112	1.02174	1.02116	1.02159	1.02245	1.02162

[a]For 14–16 band at 1221.0 cm^{-1}.

[b]For 14–16 frequencies 1300.3, 1222.7, 884.4 cm^{-1} and sites in decreasing order.

a.u. in Fig. 1). Note from the isotopic frequency ratios that these normal modes involve substantial mixing of internal coordinates.

Further evidence to support assignment of the 1300.3 and 1222.7 cm^{-1} bands to N–O stretching modes of the same species is found in the very weak 2492.0 cm^{-1} combination band observed with 3%–4% of the 1222.7 cm^{-1} band intensity in over ten metal and discharge experiments. The combination band of symmetric and antisymmetric N–O stretching modes for $(NO)_2$ is observed here at 3608.6 cm^{-1} with 6% of the 1776.2 cm^{-1} band intensity.[23] The 3608.6 cm^{-1} band becomes a 3608.6, 3979.6, and 3545.3 cm^{-1} triplet with ^{14}NO, ^{15}NO, and a 3545.3, 3503.3, and 3450.4 cm^{-1} triplet with $^{15}N^{16}O$ and $^{15}N^{18}O$. Although the 2492.0 cm^{-1} band is too weak to observe analogous triplet mixed isotopic bands, the $^{14}N^{16}O$, $^{15}N^{16}O$, and $^{15}N^{18}O$ counterparts are observed and fall 31.0, 30.1, and 28.4 cm^{-1}, respectively, below the sum of the a_1 and b_2 N–O stretching fundamentals. These differences are appropriate for normal cubic anharmonicity in the *cis*-$(NO)_2^-$ anion modes, which is 50% larger than for the analogous modes in the *cis*-$(NO)_2$ molecule.

The argon matrix absorption observed at 1364.4 cm^{-1} exhibits isotopic ratios (14–16/15–16, 1.01707; 15–16/15–18, 1.02781) near those for the diatomic N–O oscillator (1.01795 and 1.02772 for argon matrix bands). Furthermore, the argon matrix value is in excellent agreement with the neon matrix band (1369.9 cm^{-1}) tentatively assigned[8] to isolated NO^- and absorptions for the straightforward alkali metal atom-nitric oxide molecule reaction products (1353 to 1374 cm^{-1} for Li^+ to Cs^+) $(M^+)(NO)^-$ ion pairs.[5,31] If the B3LYP and reg-CASSCF calculated frequencies for NO^- (Table IV) are scaled by the NO experimental/calculated values, a NO^- frequency in the 1338–1368 cm^{-1} range is predicted. Finally, most of the gas phase electron scattering work has given NO^- frequency values in this region (1347 ± 40 cm^{-1}, for example)[32] with fairly large uncertainty, but a very recent vibrational autodetachment study reported a lower 1284 ± 10 cm^{-1} value.[33]

Several observations suggest that while the 1364.4 cm^{-1} absorption is appropriate for NO^-, it might be due to an ion cluster rather than isolated NO^-. The first is the requirement of higher NO concentrations for observation ($\geqslant 0.3\%$ in argon); the second is slight growth on 25 and 30 K annealing and slight reappearance on 30 K annealing after destruction on photolysis. Finally, higher concentrations ($\geqslant 0.8\%$) are required to clearly observe the mixed isotopic spectrum, which turns out to be a 1:1:1:1 relative intensity quartet at 1364.4, 1362.2, 1344.5, and 1341.5 cm^{-1} for the ^{14}NO and ^{15}NO mixture. This quartet indicates the minor involvement of a second inequivalent nitrogen atom and suggests that the weakly bonded $(ON)(ON)^-$ asymmetric anion cluster is the best explanation for the 1364.4 cm^{-1} absorption. Note again that this species is destroyed with visible radiation, which reduces *trans*-$(NO)_2^-$ by only 35%. This is consistent with the NO^- nature of this species, i.e., the position of the frequency, the extremely photosensitive nature of the band, and the N–O diatomic character of the vibrational mode based on isotopic ratios. Finally, this identification of the $(ON)(ON)^-$ ion cluster is supported by reg-CASSCF calculation of the $(O–N)^-$ stretching mode at 1436 cm^{-1}, which scales to 1368 cm^{-1} using the diatomic NO fundamental. The (O–N) stretching mode, calculated at 1960 cm^{-1}, is just 5 cm^{-1} lower relative to the strong NO fundamental and cannot be observed in these experiments. We believe that all of the matrix observations[5,6,8,31] point to a gas phase NO^- fundamental frequency near 1360 ± 20 cm^{-1}.

In recent neon matrix studies, structure on the low-frequency side of the 1241.5 cm^{-1} NO_2^- absorption with a prominent peak at 1227.5 cm^{-1} was attributed to NO_2^- perturbed by nearby molecules in the neon matrix.[8] These absorptions probably correspond to the 1228.1, 1222.7, and 1221.0 cm^{-1} bands observed in solid argon and characterized here as $(NO)_2^-$ species. On this basis, the extremely photosensitive 1424 cm^{-1} neon matrix band must be reassigned, and it is likely due to the less stable (presumably *cis*) isomer of $(NO)_2^+$ as only the more stable (presumably *trans*) isomer was observed here.

Reaction mechanisms

Since the reactions presented here involve NO and electrons ablated from the metal target,[34] the major route to the formation of *cis*-$(NO)_2^-$ and *trans*-$(NO)_2^-$ must be electron capture reactions as shown in reactions (1) since *cis*-$(NO)_2$ gives the strongest observed infrared absorptions:

$$cis\text{-}(NO)_2 + e^- \rightarrow [cis\text{-}(NO)_2^-]^* \xrightarrow{\text{relax}} cis\text{-}(NO)_2^- \quad (1a)$$

$$[cis\text{-}(NO)_2^-]^* \xrightarrow{\text{rearrange}} trans\text{-}(NO)_2^- \quad (1b)$$

$$[cis\text{-}(NO)_2^-]^* \xrightarrow{\text{decompose}} (ON) + (NO)^- \xrightarrow{\text{relax}} (ON)(ON)^-. \quad (1c)$$

The electron capture step is calculated to be exothermic (-2.8 eV upper bound)[18] so the energized species may relax in the matrix, rearrange to the *trans* form, or decompose to NO and NO^-. The latter will probably equilibrate back to *cis*- and *trans*-$(NO)_2^-$ if oriented ON–NO but will be trapped as an ON-ON^- complex if in the latter orientation.

There is probably some NO^- produced here but probably not much in view of the very low electron affinity of NO.[35] However, the growth of the complex $(ON)(ON)^-$ on annealing probably arises from the $ON + ON^-$ dimerization just as does the growth of $(NO)_2$ from NO dimerization.

Nitrous oxide is present here in only trace amounts, so NNO_2^- must arise from rearrangement reaction (2) and not the well-studied reaction of O^- with N_2O.[3–6,9] With lanthanide

$$cis\text{-}(NO)_2^- \text{ or } trans\text{-}(NO)_2^- \xrightarrow{\text{rearrange}} NNO_2^- \quad (2)$$

metals, reaction (2) still appears to contribute, but there is a concomitant increase in both *cis*-$(NO)_2^-$ and *trans*-$(NO)_2^-$ on photolysis, so reaction (1) must proceed followed by rearrangement to the more stable[18] *trans*-$(NO)_2^-$ (Fig. 2). In both cases 25 K annealing decreases the 1222.7 cm^{-1} site in

favor of the 1228.1 cm^{-1} site of *cis*-$(NO)_2^-$, although photolysis reverses this trend. The two ''*c*'' sites are presumed to arise from different argon packing arrangements, which may be due to formation by reaction (1a), the site favored on visible photolysis, or by $ON+NO^-$ combination, the site favored on annealing.

It is interesting to note the different relative yields of ''*c*'' and ''*t*'' and the ''*c*'' sites with different metals. While electrons are ablated from each metal target, the electromagnetic radiation is different for each metal plume, and the competing photodissociation and photodetachment processes, and the resulting populations of the anion isomers is also different for each metal.

The photolysis results in Table II are also interesting. The most photosensitive species, the complex $(ON)(ON)^-$, is bleached by visible light as it has the character of NO^- with the lowest (0.026 eV)[35] electron affinity. Note that visible photolysis also increases the more stable NO_2^- ion and increases *cis*-$(NO)_2^-$ at the expense of *trans*-$(NO)_2^-$. The latter rearrangement appears to be most efficient at 380–490 nm. Note that NNO_2^- is favored by ultraviolet (uv) photolysis as this isomer has the highest calculated vertical electron affinity (3.4 eV),[18] even higher that the electron affinity of NO_2 (2.4 eV).[36]

CONCLUSIONS

Laser ablation of metal targets with concurrent 7 or 10 K codeposition of Ar/NO mixtures produces a new 1221.0 cm^{-1} infrared absorption and a sharp 1300.3, 1222.7, and 884.4 cm^{-1} band set, which are common to aluminum and over 20 different transition and lanthanide metals. These bands decrease on annealing and on photolysis. Isotopic substitution (^{15}NO, $^{15}N^{18}O$) shows that these vibrations involve N–O oscillators, and isotopic mixtures give triplet absorption patterns for two equivalent N–O subunits, which identifies two new $(NO)_2^q$ species. The excellent agreement with frequencies, intensities, and isotopic frequency ratios from DFT/B3LYP/6-311+$G(d)$ calculations substantiates assignment of the 1221.0 cm^{-1} band to *trans*-$(NO)_2^-$ and the three band set to *cis*-$(NO)_2^-$. Broadband photolysis rearranges *cis*- and *trans*-$(NO)_2^-$ to the NNO_2^- isomer, which has a higher detachment threshold.[18]

Evidence is also presented for a new more photosensitive asymmetric $(ON)(ON)^-$ anion complex at 1364.4 cm^{-1}. Calculations at the reg-CASSCF level support this identification and predict that this complex red shifts the NO^- fundamental only 1 cm^{-1}.

ACKNOWLEDGMENTS

We gratefully acknowledge National Science Foundation (U.S.) and Swedish National Science Research Council support, and helpful correspondence with M. E. Jacox.

[1] T. R. Ward, P. Alemany, and R. Hoffman, J. Phys. Chem. **97**, 7691 (1993).
[2] J. V. Coe, J. T. Snodgrass, C. B. Freidhoff, K. M. McHugh, and K. H. Bowen, J. Chem. Phys. **87**, 4302 (1987).
[3] L. A. Posey and M. A. Johnson, J. Chem. Phys. **88**, 5383 (1988).
[4] D. W. Arnold and D. M. Newmark, J. Chem. Phys. **102**, 7035 (1995).
[5] D. E. Milligan and M. E. Jacox, J. Chem. Phys. **55**, 3404 (1971).
[6] J. Hacaloglu, S. Suzer, and L. Andrews, J. Phys. Chem. **94**, 1759 (1990).
[7] A. Strobel, N. Knoblauch, J. Agreiter, A. M. Smith, G. Neider-Schatteburg, and V. E. Bondybey, J. Phys. Chem. **99**, 872 (1995).
[8] M. E. Jacox and W. E. Thompson, J. Chem. Phys. **93**, 7609 (1990).
[9] M. E. Jacox J. Chem. Phys. **93**, 7622 (1990).
[10] L. Andrews, M. F. Zhou, and W. D. Bare J. Phys. Chem. (to be published).
[11] M. F. Zhou and L. Andrews (to be published); S. P. Willson and L. Andrews (to be published).
[12] G. P. Kushto, M. F. Zhou, L. Andrews, and C. W. Bauschlicher, Jr. (to be published).
[13] L. Andrews, T. R. Burkholder, and J. T. Yustein, J. Phys. Chem. **96**, 10182 (1992).
[14] L. Andrews, W. Saffell, and J. T. Yustein, Chem. Phys. **189**, 343 (1994).
[15] G. V. Chertihin and L. Andrews, J. Phys. Chem. **99**, 6356 (1995).
[16] G. V. Chertihin, W. Saffel, J. T. Yustein, L. Andrews, M. Neurock, A. Ricca, and C. W. Bauschlicher, Jr., J. Phys. Chem. **100**, 5261 (1996).
[17] G. V. Chertihin and L. Andrews, J. Chem. Phys. **108**, 6404 (1998).
[18] A. Snis and I. Panas, Chem. Phys. **221**, 1 (1997).
[19] A. Snis and I. Panas, Mol. Phys. **91**, 951 (1997).
[20] A. Snis and I. Panas, Surf. Sci. (to be published).
[21] K. Hiraoka, S. Fujimake, K. Aruga, and S. Yamabe, J. Phys. Chem. **98**, 8295 (1994).
[22] T. R. Burkholder and L. Andrews, J. Chem. Phys. **95**, 8697 (1991).
[23] W. A. Guillory and C. E. Hunter, J. Chem. Phys. **50**, 3516 (1969); J. F. Cantry, E. G. Stone, S. B. H. Bach, and D. W. Ball, Chem. Phys. **216**, 81 (1997).
[24] E. L. Varietti and G. C. Pimentel, J. Chem. Phys. **55**, 3813 (1971).
[25] S. Suzer and L. Andrews, J. Chem. Phys. **88**, 916 (1988).
[26] L. Andrews, G. P. Kushto, J. T. Yustein, E. Archibong, R. Sullivan, and J. Leszczynski, J. Phys. Chem. A **101**, 9077 (1997).
[27] C. Lee, W. Yang, and R. G. Parr, Phys. Rev. B **37**, 785 (1988); A. D. Becke, J. Chem. Phys. **98**, 5648 (1993).
[28] M. J. Frisch, G. W. Trucks, H. B. Schlegel, P. M. W. Gill, B. G. Johnson, M. A. Robb, J. R. Cheeseman, T. Keith, G. A. Petersson, J. A. Montgomery, K. Raghavachari, M. A. Al-Laham, V. G. Zakrzewski, J. V. Ortiz, J. B. Foresman, J. Cioslowski, B. B. Stefanov, A. Nanayakkara, M. Challacombe, C. Y. Peng, P. Y. Ayala, W. Chen, M. W. Wong, J. L. Andres, E. S. Replogle, R. Gomperts, R. L. Martin, D. J. Fox, J. S. Binkley, D. J. Defrees, J. Baker, J. P. Stewart, M. Head-Gordon, C. Gonzalez, and J. A. Pople, *Gaussian 94, Revision B. I* (Gaussian, Inc., Pittsburgh, PA, 1995).
[29] I. Panas and A. Snis, Theor. Chem. Acc. **97**, 232 (1997); K. Andersson, M. P. Fülscher, G. Karlström, R. Lindh, P. Å. Malmqvist, J. Olsen, B. O. Ross, A. Sadlej, M. R. A. Blomberg, P. E. M. Siegbahn, V. Kellö, J. Noga, M. Urban, and P.-O. Widmark, MOLCAS Version 3, Dept. of Theor. Chem., Chem. Center, University of Lund, P.O.B. 124, S-221 00 Lund, Sweden 1994.
[30] K. Pierloot, B. Dumez, P.-O. Malmqvist, and B. O. Roos, Theor. Chim. Acta **90**, 87 (1995).
[31] D. E. Tevault and L. Andrews, J. Phys. Chem. **77**, 1646 (1973).
[32] A. Zecca, I. Lazzizzera, M. Krauss, and C. E. Kuyatt, J. Chem. Phys. **61**, 4560 (1974).
[33] M. M. Maricq, N. A. Tanguay, J. C. O'Brien, S. M. Rodday, and E. Rinden, J. Chem. Phys. **90**, 3136 (1989) and references therein.
[34] R. W. Dreyfus, J. Appl. Phys. **69**, 1721 (1991).
[35] M. J. Travers, D. C. Cowles, and G. B. Ellison, Chem. Phys. Lett. **164**, 449 (1989).
[36] H. M. Rosenstock, K. Draxl, B. W. Steiner, and J. T. Herron, J. Phys. Chem. Ref. Data **68**, suppl. no. 1 (1977).